Atmos. Chem. Phys. Discuss., 10, 1559–1593, 2010
www.atmos-chem-phys-discuss.net/10/1559/2010/

Atmospheric Chemistry and Physics Discussions

This discussion paper is/has been under review for the journal Atmospheric Chemistry and Physics (ACP). Please refer to the corresponding final paper in ACP if available.

Cluster analysis of midlatitude oceanic cloud regimes – Part 1: Mean cloud and meteorological properties

N. D. Gordon[1,*] **and J. R. Norris**[1]

[1]Scripps Institution of Oceanography, University of California, San Diego, La Jolla, CA, USA
[*]now at: School of Earth and Environment, University of Leeds, Leeds, UK

Received: 17 November 2009 – Accepted: 28 December 2009 – Published: 20 January 2010

Correspondence to: N. D. Gordon (n.gordon@leeds.ac.uk)

Published by Copernicus Publications on behalf of the European Geosciences Union.

Abstract

Clouds play an important role in the climate system by reducing the amount of shortwave radiation reaching the surface and the amount of longwave radiation escaping to space. Although dependent on type and location, clouds produce more cooling than warming in the global average. Accurate simulation of clouds in computer models remains elusive, however, pointing to a lack of understanding of the connection between large-scale dynamics and cloud properties. This study uses a *k*-means clustering algorithm to group 21-years of satellite cloud data over midlatitude oceans into seven clusters and demonstrates that the cloud clusters are associated with distinct large-scale dynamical conditions. Three clusters correspond to low-level cloud regimes with different cloud fraction and cumuliform or stratiform characteristics, but all occur under large-scale descent and a relatively dry free troposphere. The "small cumulus" regime is most prevalent equatorward of 40° in all seasons; the "large cumulus" regime is associated with a relatively cold troposphere and primarily occurs during winter; and the "stratocumulus/stratus" regime occurs under a temperature inversion and relatively warm free troposphere and predominates during summer. Three clusters correspond to vertically extensive cloud regimes with tops in the middle or upper troposphere. They differ according to the strength of large-scale ascent and enhancement of tropospheric temperature and humidity: "deep altostratus" has the smallest forcing, "weak frontal" is in the middle, and "strong frontal" has the largest forcing. The frontal cloud regimes occur most frequently in storm track regions. The final cluster, "cirrus" is associated with a lower troposphere that is dry and an upper troposphere that is moist and experiencing weak ascent and horizontal moist advection. This information builds a foundation for producing an observational estimate of the midlatitude ocean cloud response to warming that is independent of confounding meteorological influences.

ACPD

10, 1559–1593, 2010

1 Introduction

The representation of clouds in climate models continues to be the largest source of uncertainty in simulations of future climate. Much of the inter-model variability in equilibrium surface temperature change for doubled carbon dioxide scenarios is due to differences in the way that clouds are represented within the models (IPCC, 2007). Many past studies of model fidelity focused on large spatial and temporal scales (e.g., Weare et al., 1996; Zhang et al., 2005), but averaging across disparate dynamical regimes can mask the presence of compensating errors. For example, Norris and Weaver (2001) found that overprediction of cloud fraction during conditions of upward motion in the National Center for Atmospheric Research (NCAR) Community Climate Model Version 3 (CCM3) was largely compensated by underprediction of cloud fraction during conditions of downward motion. This study, along with others (e.g., Klein and Jakob; Tselioudis and Jakob, 2002), illustrated the utility of compositing on meteorological parameters, whereby cloud scenes are grouped according to one or more selected dynamical and thermodynamical properties of the atmosphere. Dividing the atmosphere into a series of distinct meteorological regimes, each with different cloud properties, is an effective method for understanding the connections between the dynamics and thermodynamics of the atmosphere and the clouds they produce (Jakob, 2003).

Recent studies have used clustering algorithms to identify cloud regimes without direct reference to meteorological parameters (e.g., Gordon et al., 2005; Rossow et al., 2005). This approach, first proposed for this use by Jakob and Tselioudis (2003), provides a more objective means of categorizing clouds and has the additional advantage of not requiring prior knowledge of the large-scale meteorological processes important for cloud formation. For example, Gordon et al. (2005) found that six distinct cool-season cloud clusters for the southern Great Plains region did not exhibit simple unique relationships with midtropospheric vertical velocity (e.g., the assumption of Norris and Weaver, 2001). Different cloud clusters were instead associated with different

ACPD
10, 1559–1593, 2010

vertical profiles of vertical motion and horizontal moisture advection. Identifying the specific vertical distribution of dynamical and thermodynamical processes generating a particular type of cloud is crucial for understanding the atmosphere and improving model simulation of clouds.

The present study extends the clustering approach of Gordon et al. (2005) to all midlatitude ocean grid boxes. Only ocean regions are examined so as to minimize the role that surface features play in cloud forcing. We use a *k*-means clustering algorithm to classify daily grid box cloud data from the International Satellite Cloud Climatology Project (ISCCP) into seven groups according to similar cloud fraction values in three cloud top pressure intervals and three cloud optical thickness intervals. Vertical profiles of reanalysis relative humidity, temperature, vertical velocity, horizontal temperature advection, and horizontal moisture advection are averaged over each cluster as perturbations from the mean state. This provides insight into meteorological conditions and dynamical forcing associated with each cloud regime, which is supplemented by examination of the climatological distribution and seasonal cycle of each cluster.

These results will provide a foundation for subsequent investigation of the sensitivity of cloud properties to changes in temperature independent from dynamical forcing. Bony et al. (2004) proposed a method for distinguishing dynamical and thermodynamical influences on cloud properties by examining how clouds changed with temperature for narrow ranges of a dynamical parameter. Clustering is a useful tool for this purpose because it groups cloud types with similar meteorology, and Williams and Tselioudis (2007) employed it to examine the relative contribution of changes to cloud properties to due to dynamic and thermodynamic changes in GCMs. In a companion paper (Part 2) to this study, we extend our analysis to examine how cloud properties change with temperature within each cluster as lapse rate, horizontal temperature advection, and vertical temperature advection are held constant.

ACPD
10, 1559–1593, 2010

2 Data sources

The source of cloud observations for this investigation was the three-hourly International Satellite Cloud Climatology Project (ISCCP) D1 equal-area (280 km×280 km) data set, originally processed from radiances primarily measured by geostationary weather satellites (Rossow et al., 1996; Rossow and Schiffer, 1999). The ISCCP data consist of cloud fractions within a gridbox for nine categories of cloudiness based on three intervals of cloud-top pressure (CTP) (below 680 mb, between 680 and 440 mb, and above 440 mb) and three intervals of cloud optical thickness (τ) (between 0.3 and 3.6, between 3.6 and 23, and above 23). Since cloud optical thickness values are obtained from visible retrievals, valid data only exist for daytime hours. We restricted our analysis to one time point per day for each satellite gridbox, choosing the value with the smallest solar zenith angle (closest to local noon). This restriction avoided sampling biases associated with more valid data points coming from regions near the equator and from points in the summer hemisphere, where there are a greater number of daylight hours. The satellite pixels used to generate the CTP-τ histograms are approximately 4–7 km in size and spaced approximately 30 km apart, with up to 80 pixels per gridbox.

Our analysis spans nearly the entire available record of ISCCP, 21 years (1984–2004), and incorporates all ocean points between 30° and 50° in both hemispheres, representing 1444 gridboxes. The ISCCP data consisted of nearly 10 million CTP-τ histograms over all days and grid boxes. The CTP-τ histogram corresponds to a nine-type cloud fraction array. All values of the nine-type cloud fraction array are exactly zero for clear-sky observations, which infrequently occur (less than 1% of the total number of days and grid boxes) and are excluded from the clustering.

In addition to mean cloud properties, we examined the radiative flux data derived from the ISCCP data (Zhang et al., 2004). The flux data consists of upwelling and downwelling, shortwave and longwave radiative flux for both clear and cloudy parts of the gridbox. This data is provided at the surface, the top of the atmosphere (TOA), and at three levels within the atmosphere (680 mbar, 440 mbar, and 100 mbar). To

ACPD
10, 1559–1593, 2010

complement the satellite-derived properties of the cloud regimes, we also analyzed surface-based visual cloud type observations from the Extended Edited Cloud Report Archive (EECRA) (Hahn and Warren, 1999).

We obtained information about the dynamics and thermodynamic structure of the atmosphere from the National Center for Environmental Prediction (NCEP) NCAR Reanalysis (Kalnay et al., 1996). This data set provided standard meteorological parameters as well as information about large-scale gradients and atmospheric motions that were needed to calculate the advective tendencies of moisture and temperature, which are important to cloud formation and dissipation. We have restricted our analysis to middle latitudes because that is where much of the dynamical forcing that leads to cloud formation in these regions is at or above the spatial scale of the satellite grid boxes and vertical motion in the NCEP-NCAR reanalysis is best-constrained by observations.

3 Cluster analysis method

The ISCCP cloud data were grouped into regimes by applying a k-means clustering algorithm to the nine-type cloud fraction arrays (CTP-τ histograms). The k-means procedure classifies all nine-type arrays into a specified number of clusters such that within-cluster variance is minimized (Hartigan, 1975; Jakob and Tselioudis, 2003). The only arbitrary parameter needed is the number of clusters; the character of the individual cluster means is then objectively determined by the data. The clustering process began with random selection of k nine-type arrays as initial seeds. All other nine-type arrays in the data set were then assigned to the initial seed to which they were closest in a Euclidean sense. The number of nine-type arrays in a cluster divided by the total number of nine-type arrays is the frequency of occurrence of the cluster, and the average of all nine-type arrays in the cluster is the centroid (e.g., average cloud fraction for each of the nine CTP-τ categories). These cluster centroids became new seeds to reinitialize the clustering routine, which was repeated until the centroids converged.

ACPD
10, 1559–1593, 2010

An uncertainty in the k-means method is the convergence of the clustering algorithm to different results for different initial seeds. We resolved this ambiguity by clustering on 50 different sets of random initial seeds and choosing the final cluster set with the least sum of variance around each cluster centroid (the other possible solutions will be discussed later). Specifying the number of clusters is the most subjective aspect of the k-means method. After examining results for various numbers, we chose to use seven clusters, as that was the minimum number of clusters that had clearly distinct cloud properties and meteorological conditions. Additional clusters beyond seven overlapped preceding clusters without providing appreciable new information; inclusion of such intermediate clusters would have increased the number of plots without commensurately enhancing our understanding of dynamical and thermodynamical conditions associated with particular cloud regimes.

Our approach differs from that of Gordon et al. (2005) in that we cluster on cloud fraction in nine CTP-τ categories rather than gridbox mean cloud fraction, cloud-top pressure, and cloud reflectivity. We instead took the approach used by Jakob and Tselioudis (2003), except that they used 42 CTP-τ categories (cloud fraction within each of seven CTP and six τ intervals). Because cloud fraction in 42 CTP-t categories did not provide significantly more information, we aggregated the 42 categories into nine categories that correspond to the standard ISCCP-defined cloud types.

4 Cloud properties

Table 1 lists mean cloud fraction, CTP, τ, and cloud top temperature averaged over all CTP-τ categories for the cluster centroids during the 1984–2004 time period, ordered according to relative frequency. The nonlinear relationship between radiation flux and optical thickness was taken into account by converting cloud optical thickness values to cloud reflectivity at 0.6 microns using an ISCCP look-up table (corresponding to Fig. 3.13 in Rossow et al., 1996) before averaging. The mean reflectivity was then converted back to cloud optical thickness using the same table. This ensures that

ACPD
10, 1559–1593, 2010

our cluster mean optical thickness values more correctly represent cloud effects on gridbox-mean visible radiation flux.

Table 2 lists mean TOA shortwave cloud radiative forcing (SWCRF) and longwave cloud radiative forcing (LWCRF) for each of the clusters. These are diurnal mean values calculated from near-noon values according to the method described in the Appendix. Following Ramanathan et al. (1989), we define cloud radiative forcing as outgoing radiative flux for all-sky conditions subtracted from outgoing radiative flux for cloud-free conditions. Thus, SWCRF values are negative and represent a net cooling of the climate system, and LWCRF values are positive and represent a net warming of the climate system. Reasons for the informal names given to each cluster in Tables 1 and 2 will be described in the following paragraphs.

As a complement to the satellite observations, we examined cloud information reported by surface observers on ships in the same grid box and on the same day as the ISCCP data. These provide a bottom-up view of the scene along with morphological rather than radiative characterizations of cloud types and precipitation (for a non-technical description of low-level cloud types, see Table 1 of Norris, 1998a). Table 3 lists average surface-observed total cloud cover and low-level cloud cover for each cluster together with the frequencies at which surface observers report the occurrence of clear sky, sky obscuration by fog or precipitation, non-drizzle precipitation, various low-level cloud types, and the absence of low-level cloudiness. In order to distinguish relative differences between clusters more easily, anomalies from the frequency-weighted mean across all clusters are provided. Because ship sampling is sparse over Southern Hemisphere midlatitude oceans, Table 3 includes only Northern Hemisphere points. This should not bias the results appreciably since no cluster is primarily restricted to the Southern Hemisphere, and mean cloud properties and dynamics are similar for each cluster in either hemisphere (not shown). There is general agreement but not exact correspondence between Tables 1 and 3 due to the different spatial scale and method of satellite and surface observations.

ACPD
10, 1559–1593, 2010

Figure 1 displays the mean cloud fraction for all categories in the ISCCP CTP-τ histograms for each of the seven clusters. If mean cloud fraction in a category is less than 2%, it is not displayed. The three most frequent clusters all correspond to low-level cloud regimes, as seen by the predominance of clouds with CTP greater than 680 mb. Since surface observers report small cumulus and clear sky more frequently for Cluster 1 than any other cluster (Table 3), we will refer to it as the "small cumulus" cluster. We call Cluster 2 "large cumulus" and Cluster 3 "stratocumulus/stratus" for the similar reasons. Cluster 1 has the smallest cloud fraction of all clusters, and low-level and total cloud fraction increase from Cluster 1 to 2 to 3 (Tables 1 and 3), consistent with their "Small Cu", "Large Cu", and "Sc/St" designations. Clusters 1, 2, and 3 have weak LWCRF (Table 3) because their low cloud tops are relatively warm (Table 1). Cluster 3 has stronger SWCRF than do Clusters 1 and 2, as would be expected for horizontally extensive stratiform cloud.

Cluster 4 is the only cluster with a cloud top in the middle troposphere (Fig. 1). The large low-level cloud amount and stratiform cloud types very frequently reported by surface observers for this cluster (Table 3) suggests that these clouds usually extend from the middle troposphere down to near the surface, even though the satellite retrievals are unable to provide that information. For this reason, we call Cluster 4 "deep altostratus". Table 2 shows that it has larger LWCRF than the low-level cloud clusters and relatively strong SWCRF.

The last three clusters in Fig. 1 are high-top cloud regimes with optical thickness that increases from Cluster 5 to 6 to 7. We call Cluster 5 "cirrus" because it has the smallest optical thickness and greatest absence of low-level cloud of all clusters (Tables 1 and 3). The magnitude of SWCRF is only slightly larger than the magnitude of LWCRF for Cluster 5 (Table 2), which is the only case where the cooling from reflected solar radiation is nearly cancelled out by the trapping of longwave radiation emitted by the surface. Clusters 6 and 7 contrastingly have a large cooling effect on climate because their very negative SWCRF substantially outweighs their large positive LWCRF. As was the case for Cluster 4, surface observers report large low-level cloud amount

ACPD
10, 1559–1593, 2010

by stratiform types, indicating that Clusters 6 and 7 have vertically extensive clouds. Surface observers also report the occurrence of precipitation 13% of the time for Cluster 6 and 30% of the time for Cluster 7 (Table 3). We call Cluster 6 "weak frontal" and Cluster 7 "strong frontal". The net CRF values (e.g., SWCRF+LWCRF) for the "weak frontal" and "strong frontal" regimes are −81 and −45 W/m^2, respectively, consistent with the approximate −70 W/m^2 value reported by Weaver and Ramanathan (1996) for midlatitude ocean synoptic storms. Averaging over all clusters with weighting by their relative frequencies, we calculate a net CRF cooling of −39 W/m^2 by midlatitude ocean clouds.

As mentioned previously, our clustering algorithm may converge to a different solution, depending on the initial seeds provided. We resolved this by taking the solution with the smallest total variance. Besides the solution presented in Fig. 1, there are two additional sets of clusters to which the solution can converge. The only difference is the inclusion of either another low-level cloud or midlevel cloud cluster, both which occur with the loss of one of the frontal clusters. In analyzing clustering results for values of k greater than seven, we often found cases with more than three low-level cloud or more than one midlevel cloud cluster. In both of these instances, the inclusion of the additional cluster did not provide any additional information since the cluster with intermediate cloud properties also exhibited intermediate meteorological properties.

5 Characteristic dynamics

To provide insight into the atmospheric state and advective forcing associated with the various cloud regimes, we averaged vertical profiles of NCEP/NCAR Reanalysis data over the grid boxes and times corresponding to each cluster. Monthly means for each spatial point and each vertical level were removed from all meteorological parameters to prevent spatial and seasonal biases from affecting the results. Thus, meteorological conditions associated with the clusters will represent perturbations from the mean state. The advective tendencies of water-vapor mixing ratio were converted to

ACPD
10, 1559–1593, 2010

tendencies in relative humidity (RH) by dividing by the saturation mixing ratio at each level. For consistency, we chose all values of RH and saturation with respect to liquid water even though saturation with respect to ice may be more applicable in the upper troposphere. Additionally, the meridional wind for all points in the Southern Hemisphere was multiplied by −1 before averaging so that positive horizontal flow is in a poleward sense. Vertical profiles of perturbation RH are displayed in Fig. 2, perturbation temperature in Fig. 3, perturbation pressure vertical velocity in Fig. 4, perturbation horizontal advective tendencies of water-vapor mixing ratio in Fig. 5, and perturbation horizontal advective tendencies of temperature in Fig. 6. Profiles of vertical advection tendencies of both temperature and water vapor (not shown) are similar to the profile of vertical motion (water vapor being the opposite sign).

The mean cloud properties of each cluster are physically consistent with the meteorological state and dynamical forcing. The low-level cloud Clusters (1, 2, and 3) occur with negative perturbation RH in the middle and upper troposphere (Fig. 2) that is produced by grid box mean vertical descent (Fig. 4). Cluster 1 (Small Cu) has the weakest average dynamical forcing, with near-mean profiles in temperature (Fig. 3), zonal and meridional wind (not shown), horizontal advection of moisture (Fig. 5), and horizontal advection of temperature (Fig. 6). Clusters 2 and 3 have similar dynamics (downward motion and low-level horizontal advective perturbation drying and cooling), but their temperature profiles are quite different. Cluster 2 (Large Cu) occurs with a relatively cold boundary layer and cold free troposphere, whereas Cluster 3 (Sc/St) occurs with a relatively cool boundary layer and relatively warm free troposphere (thus indicating a perturbation temperature inversion). These characteristics are consistent with the vertical temperature profile and dynamical processes previously found to be associated with surface-observed midlatitude large cumulus and stratocumulus, respectively (Norris, 1998a; Norris and Klein, 2000). In the Large Cu cluster, perturbation temperature switches from cold below 300 mb to warm above 300 mb, suggesting a depressed tropopause. Contrastingly, the Sc/St cluster has an opposite temperature reversal – warm below and cold above 300 mb, suggesting a slightly elevated tropopause (Fig. 3).

ACPD
10, 1559–1593, 2010

Clusters 6 (Weak Frontal) and 7 (Strong Frontal) appear to occur east of the trough and west of the ridge in a midtropospheric synoptic wave. Both occur with strong upward motion (Fig. 4) and a very moist troposphere (Fig. 2). Although not shown, perturbation horizontal velocity in the upper troposphere is southwesterly (in a Northern Hemisphere sense), which is consistent with the positive perturbation temperature advection (Fig. 6), warm tropospheric temperature, and elevated tropopause (Fig. 3). Figure 5 indicates that both frontal clusters have horizontal perturbation moistening in the lower troposphere, and the strong upward moisture advection clearly dominates the horizontal perturbation drying in the upper troposphere to create vertically extensive cloudiness. Consistent with the names of the clusters, the Weak Frontal cluster has smaller perturbations in meteorological state and dynamical forcing than the Strong Frontal cluster. Cluster 4 (Deep As) exhibits vertical profiles of perturbation RH, temperature, vertical velocity, horizontal temperature advection, and horizontal moisture advection that have similar shapes and signs, albeit with much weaker magnitude, to those of the frontal clusters.

The RH profile for Cluster 5 (Cirrus) shows negative perturbation moisture below 600 mb and significant positive perturbation moisture above 600 mb (Fig. 2), and the negative temperature perturbation above 250 mb (Fig. 3) suggests that it coincides with an elevated tropopause. The large positive horizontal perturbation moisture advection (Fig. 5) suggests that some of these clouds are blow-off from a deep convective system or an extratropical cyclone, and the small upward motion in the upper troposphere suggests that some of these clouds may be locally dynamically generated (Fig. 4).

In addition to looking at the local meteorological conditions, we can examine the spatial relationships between cloud regimes corresponding to each cluster. This can be accomplished by compositing the frequency of occurrence of various clusters in grid boxes surrounding a central point (e.g., Lau and Crane, 1995; Norris and Iacobellis, 2005; among others). In this case we choose as a central point those grid boxes in which the Strong Frontal cluster is present. To avoid biases from geographical and seasonal variations in cluster distribution, we subtracted the long-term monthly

ACPD
10, 1559–1593, 2010

mean cluster frequency for each grid box before adding it to the composite. Figure 7 shows the results, which are generally consistent with the placement of cloud regimes in a midlatitude synoptic wave. By construction, there is a large positive perturbation in the frequency of Cluster 7 (Strong Frontal) at the center of the composite. Cluster 6 (Weak Frontal) is also relatively frequent in the region surrounding the center, especially to the northeast (in a Northern Hemisphere sense). The frequency of Cluster 5 (Cirrus) is enhanced equatorward and eastward (e.g., ahead) of the frontal regime. Clusters 1 (Small Cu) and 2 (Large Cu) more frequently occur northwest of the frontal regime (e.g., in the cold sector).

6 Spatial distribution and seasonal cycle

Figure 8a–g shows the spatial distribution of the annual mean frequency of each cluster. Note that some artificial features associated with the viewing geometry of geostationary satellites are present and do not reflect real geographical variations (Rossow and Garder, 1993). The overall most frequent cluster, Small Cu, predominantly occurs in equatorward and coastal regions of our domain (Fig. 8a), as may be expected for the cluster with the least cloud fraction and greatest prevalence of surface-reported cumuliform cloud types (Table 3 of this study; Figs. 5 and 6 of Norris, 1998b). The CTP-τ histogram for Small Cu (Fig. 1) shows that this cluster is primarily composed of low-level clouds, but some small amount of higher clouds is mixed in, as implied by the lower grid box mean CTP for this cluster relative to the other low-level cloud clusters (Table 1). The second cluster, Large Cu, occurs more often in the center of the ocean basins and is more prevalent in the Southern Hemisphere (Fig. 8b). The final low-level cloud cluster, Sc/St, has a very distinctive geographical distribution. The region of highest frequency is the subtropical anticyclone region in the eastern Pacific Ocean, and other regions of frequent Sc/St include the far northern Pacific Ocean and off the west coast of Australia (Fig. 8c). Other climatological subtropical stratocumulus regions are too far equatorward to be included in our analysis (Norris, 1998b).

ACPD
10, 1559–1593, 2010

The only predominantly midlevel cluster, Deep As, is primarily located in the higher latitude regions of the analysis domain (Fig. 8d). Cluster 5 (Cirrus) is most frequent immediately east of continents (South America, North America, and Southern Africa). Another region of increased frequency is in the central Pacific, possibly due to advection from the deep convective towers of the west Pacific equatorial warm pool (Fig. 8e). The final two clusters (Weak Frontal and Strong Frontal) are fixtures of the storm track, with the Strong Frontal cluster more focused in the western half of the ocean basins (Fig. 8f–g).

Williams and Tselioudis (2007) (hereafter WT07) performed a similar study by clustering ISCCP histograms for the ice-free extratropics (poleward of 20° in both hemispheres). Although they only examine five cloud clusters, their results are very similar to those produced from our analysis (Fig. 6 from WT07). The WT07 clusters of shallow cumulus, stratocumulus, cirrus, mid-level, and frontal are similar to Small Cu, Sc/St, Cirrus, Deep As, and Strong Frontal (respectively). The WT07 study examined a much larger domain, allowing points poleward of 55°, provided that they are ice-free, more subtropical points, and points over land.

In order to gain a more in-depth understanding of the relationship of each cluster to large-scale dynamical processes, it is useful to examine the seasonal cycle of each cluster's spatial distribution. For Cluster 1 (Small Cu), the spatial distribution of each season is nearly identical to that of the annual mean and is therefore not shown. Figure 9a and b displays the spatial distribution of Cluster 2 (Large Cu) for the December-January-February (DJF) and June-July-August (JJA) seasons, respectively. This cloud regime predominantly occurs in the winter season, suggesting that these clouds are the result of cold air advecting over warmer water behind a frontal system (Fig. 7). Cluster 3 (Sc/St) also has a very strong seasonal cycle (Fig. 10a and b), but unlike Cluster 2, it primarily occurs during the summer season. Stratocumulus clouds in the eastern Pacific anticyclone region and stratus clouds in the central North Pacific are most extensive during JJA (Norris, 1998b).

ACPD
10, 1559–1593, 2010

The spatial distribution of Cluster 4 (Deep As) frequency for each season is fairly similar to the mean distribution (not shown). One large exception is the North Pacific during JJA, where Deep As is especially prevalent (Fig. 11). The restriction of this cloud regime to higher latitudes and its increased frequency in Northern Hemisphere summer suggests that these are weakly forced and shallow synoptic storms. Surface observers report precipitation for the Deep As cluster nearly as often as they do for the Weak Frontal cluster (Table 3). Cluster 5 (Cirrus) also has little seasonality for the most part. One exception is that the frequency of Cirrus is enhanced in the western North Pacific Ocean near the southern boundary of our domain during JJA (Fig. 12). These high-level clouds may be the result of greater nearby convection in the western tropical warm pool.

7 Conclusions

This study demonstrates how midlatitude oceanic clouds can be grouped into distinct regimes based on a *k*-means clustering algorithm applied to satellite-derived cloud fraction in three intervals of cloud-top pressure and three intervals of cloud optical thickness. Surface observations of cloud cover and morphological cloud type helped us interpret the radiatively-based satellite cloud data and determine the vertical extent of clouds with high tops. Atmospheric dynamical and thermodynamical information, obtained from the NCEP/NCAR Reanalysis, enabled us to examine the synoptic environment and advective tendencies associated with the cloud regimes. The climatological spatial distribution and seasonal cycle of the frequencies of occurrence for each cluster were consistent with dynamical processes generating each cloud regime.

Clusters 6 and 7 (Weak Frontal and Strong Frontal, respectively) have vertically extensive clouds with tops in the upper troposphere. They are associated with meteorological conditions indicative of being east of a trough in an upper-level synoptic wave: strong ascent, southwesterly flow, enhanced moisture throughout the troposphere, relatively warm temperature, and an elevated tropopause. These cloud regimes are

ACPD
10, 1559–1593, 2010

climatologically most frequent in storm track regions and preferentially occur in the winter season. The low-level cloud clusters (1 – Small Cu, 2 – Large Cu, and 3 – Sc/St) are associated with weak descent, a dry upper troposphere, and relatively cool and dry horizontal advective tendencies, consistent with the expected dynamical conditions that would be associated with low-level clouds over the ocean. Cluster 2 (Large Cu) is climatologically most frequent during winter and occurs with a relatively cold temperature throughout the troposphere. Cluster 3 (Sc/St) contrastingly is climatologically most frequent during summer and occurs with a temperature inversion under a relatively warm free troposphere. Cluster 1 (Small Cu) is climatologically most frequent equatorward of 40° and exhibits little seasonal cycle. One of the remaining clusters, 5 – Cirrus, is most common east of continents and occurs with a dry lower troposphere and a moist upper troposphere produced by horizontal advective moistening and weak ascent. The last cluster, 4 – Deep As, is the only cloud regime with a top in the middle troposphere. It is most common poleward of 50° and resembles the frontal clusters, albeit with substantially smaller magnitude.

Clustering is a useful tool for examining large amounts of data and extracting information about patterns within the data. Although our clustering was based solely on cloud properties, the resulting clusters were associated with physically consistent large-scale dynamics. Moreover, we did not need to assume a priori what meteorological processes exerted the most control over various cloud regimes. These results will be an effective method of diagnosing the ability of GCMs to accurately simulate clouds. Additionally, since within each cluster there are relatively similar dynamics, we can better investigate the impact of changes in atmospheric temperature on cloud properties (Part 2). By constraining dynamical forcing constant, we will be able to obtain an estimate of the partial derivative of cloud properties with respect to temperature from observations rather than from computer models, thus improving our understanding of cloud feedbacks on climate.

ACPD
10, 1559–1593, 2010

Appendix A

Ramanathan et al. (1989) defined cloud radiative forcing as the difference in the radiative flux between all-sky conditions and cloud-free conditions at the top of the atmosphere (TOA), for both shortwave (SWCRF) and longwave radiation (LWCRF):

$$\mathrm{SWCRF} = \left(\mathrm{SW}\uparrow^{\mathrm{TOA}}_{\mathrm{clear}} - \mathrm{SW}\uparrow^{\mathrm{TOA}}_{\mathrm{all\text{-}sky}}\right) \tag{A1}$$

$$\mathrm{LWCRF} = \left(\mathrm{LW}\uparrow^{\mathrm{TOA}}_{\mathrm{clear}} - \mathrm{LW}\uparrow^{\mathrm{TOA}}_{\mathrm{all\text{-}sky}}\right) \tag{A2}$$

Here, SW and LW refer to the shortwave and longwave, respectively, flux of radiation, for either clear or all-sky conditions. For this equation, we are only interested in the upwelling component of the radiative flux. The ISCCP cloud data we used are from the 3-hourly observation closest to local noon, the time of day when downwelling shortwave radiation at TOA and the upwelling longwave radiation at the surface are diurnal maximums and have large variability over season and location. In order to avoid a radiative weighting that would bias towards summertime and low-latitude points, we normalize our radiation parameters by the downwelling SW at TOA for SWCRF and by the upwelling LW radiation at the surface. Thus our cloud radiative forcing parameters become:

$$\mathrm{SWCRF}_{\mathrm{norm}} = \left(\mathrm{SW}\uparrow^{\mathrm{TOA}}_{\mathrm{clear}} - \mathrm{SW}\uparrow^{\mathrm{TOA}}_{\mathrm{all\text{-}sky}}\right) \Big/ \left(\mathrm{SW}\downarrow^{\mathrm{TOA}}\right) \tag{A3}$$

$$\mathrm{LWCRF}_{\mathrm{norm}} = \left(\mathrm{LW}\uparrow^{\mathrm{TOA}}_{\mathrm{clear}} - \mathrm{LW}\uparrow^{\mathrm{TOA}}_{\mathrm{all\text{-}sky}}\right) \Big/ \left(\mathrm{LW}\uparrow^{\mathrm{surface}}\right) \tag{A4}$$

To get a diurnal average of the cloud forcing in units of $\mathrm{W/m^2}$, as opposed to a noontime value, we multiplied the normalized cloud forcing by the diurnally averaged value of downwelling shortwave flux at TOA for $\mathrm{SWCRF}_{\mathrm{norm}}$ or the upwelling longwave flux

ACPD
10, 1559–1593, 2010

at the surface for $LWCRF_{norm}$. Both of these values were determined by averaging the ISCCP flux data for all three-hourly data points during a day, yielding:

$$SWCRF_{diurnal} = SW\downarrow^{TOA}_{diurnal}\left(SW\uparrow^{TOA}_{clear} - SW\uparrow^{TOA}_{all\text{-}sky}\right) \Big/ SW\downarrow^{TOA} \quad \text{(A5)}$$

$$LWCRF_{diurnal} = LW\uparrow^{surface}_{diurnal}\left(LW\uparrow^{TOA}_{clear} - LW\uparrow^{TOA}_{all\text{-}sky}\right) \Big/ LW\uparrow^{surface} \quad \text{(A6)}$$

Acknowledgements. This work was supported by NSF CAREER Grant AM02-38257 and NASA Grant GWEC NAG5-11731.

References

Bony, S., Dufresne, J.-L., Le Treut, H., Morcrette, J.-J., and Senior, C.: On dynamic and thermodynamic components of cloud changes, Clim. Dynam., 22, 71–86, 2004.

Gordon, N. D., Norris, J. R., Weaver, C. P., and Klein, S. A.: Cluster analysis of cloud regimes and characteristic dynamics of midlatitude synoptic systems in observations and a model, J. Geophys. Res., 110, D15S17, doi:10.1029/2004JD005027, 2005.

Hahn, C. J. and Warren, S. G.: Extended Edited Cloud Reports from Ships and Land Stations over the Globe, 1952–1996. Numerical Data Package NDP-026C, Carbon Dioxide Information Analysis Center (CDIAC), Department of Energy, Oak Ridge, Tennessee, 79 pp., 1999.

Hartigan, J. A.: Clustering Algorithms, Wiley Press, New York, NY, 351 pp., 1975.

IPCC Climate Change 2007: The Physical Science Basis, Contribution of Working Group I to the Fourth Assessment Report of the Intergovernmental Panel on Climate Change, edited by: Solomon, S., Qin, D., Manning, M., Chen, Z., Marquis, M., Averyt, K. B., Tignor, M., and Miller, H. L., Cambridge University Press, Cambridge, UK and New York, NY, USA, 996 pp., 2007.

Jakob, C.: An improved strategy for the evaluation of cloud parameterizations in GCMs, B. Am. Meteorol. Soc., 84, 1387–1401, 2003.

Jakob, C. and Tselioudis, G.: Objective identification of cloud regimes in the Tropical West Pacific, Geophys. Res. Lett., 30(21), Art. No. 2082, 2003.

Jakob, C., Tselioudis, G., and Hume, T.: The radiative, cloud and thermodynamic properties of the major Tropical Western Pacific cloud regimes, J. Climate, 18, 1203–1215, 2005.

Kalnay, E., Kanamitsu, M., Kistler, R., Collins, W., Deaven, D., Gandin, L., Iredell, M., Saha, S., White, G., Woollen, J., Zhu, Y., Chelliah, M., Ebisuzaki, W., Higgins, W., Janowiak, J., Mo, K. C., Ropelewski, C., Wang, J., Leetmaa, A., Reynolds, R., Jenne, R., and Joseph, D.: The NCEP/NCAR 40-year reanalysis project, B. Am. Meteorol. Soc., 77, 437–470, 1996.

Klein, S. A. and Jakob, C.: Validation and sensitivities of frontal clouds simulated by the ECMWF model, Mon. Weather Rev., 127, 2514–2531, 1999.

Lau, N.-C. and Crane, M. W.: A satellite view of the synoptic-scale organization of cloud cover in midlatitude and tropical circulation systems, Mon. Weather Rev., 123, 1984–2006, 1995.

Norris, J. R.: Low cloud type over the ocean from surface observations, Part I: Relationship to surface meteorology and the vertical distribution of temperature and moisture, J. Climate, 11, 369–382, 1998a.

Norris, J. R.: Low cloud type over the ocean from surface observations, Part II: Geographical and seasonal variations, J. Climate, 11, 383–403, 1998b.

Norris, J. R. and Klein, S. A.: Low cloud type over the ocean from surface observations, Part III: Relationship to vertical motion and the regional surface synoptic environment, J. Climate, 13, 245–256, 2000.

Norris, J. R. and Weaver, C. P.: Improved techniques for evaluating GCM cloudiness applied to the NCAR CCM3, J. Climate, 14, 2540–2550, 2001.

Norris, J. R. and Iacobellis, S. F.: North Pacific cloud feedbacks inferred from synoptic-scale dynamic and thermodynamic relationships, J. Climate, 18, 4862–4878, 2005.

Ramanathan, V., Barkstrom, B. R., and Harrison, E. F.: Climate and the earth's radiation budget, Phys. Today, 42(5), 22–33, 1989.

Rossow, W. B. and Garder, L. C.: Validation of ISCCP cloud detections, J. Climate, 6, 2370–2393, 1993.

Rossow, W. B., Walker, A. W., Beuschel, D. E., and Roiter, M. D.: International Satellite Cloud Climatology Project (ISCCP) Documentation of New Cloud Datasets, WMO/TD-No. 737, World Meteorological Organization, 115 pp., 1996.

Rossow, W. B. and Schiffer, R. A.: Advances in understanding ISCCP, B. Am. Meteorol. Soc., 80, 2261–2287, 1999.

Rossow, W. B., Tselioudis, G., Polak, A., and Jakob, C.: Tropical climate described as a distribution of weather states indicated by distinct mesoscale cloud property mixtures, Geophys. Res. Lett., 32, L21812, doi:10.1029/2005GL024584, 2005.

ACPD

10, 1559–1593, 2010

Tselioudis, G. and Jakob, C.: Evaluation of midlatitude cloud properties in a weather and a climate model: dependence on dynamic regime and spatial resolution, J. Geophys. Res., 107, 4781, doi:10.1029/2002JD002259, 2002.

Weare, B. C. and AMIP Modeling Groups: Evaluation of the vertical structure of zonally averaged cloudiness and its variability in the atmospheric model intercomparison project, J. Climate, 9, 3419–3431, 1996.

Weaver, C. P. and Ramanathan, V.: The link between summertime cloud radiative forcing and extratropical cyclones in the N. Pacific, J. Climate, 9, 2093–2109, 1996.

Williams, K. D. and Tselioudis, G.: GCM intercomparison of global cloud regimes: present-day evaluation and climate change response, Clim. Dynam., 29, 231–250, 2007.

Zhang, Y., Rossow, W. B., Lacis, A. A., Oinas, V., and Mishchenko, M. I.: Calculation of radiative fluxes from the surface to top of atmosphere based on ISCCP and other global data sets: refinements of the radiative transfer model and the input data, J. Geophys. Res., 109, D19105, doi:10.1029/2003JD004457, 2004.

Zhang, M. H., Lin, W. Y., Klein, S. A., Bacmeister, J. T., Bony, S., Cederwall, R. T., Del Genio, A. D., Hack, J. J., Loeb, N. G., Lohmann, U., Minnis, P., Musat, I., Pincus, R., Stier, P., Suarez, M. J., Webb, M. J., Wu, J. B., Xie, S. C., Yao, M.-S., and Zhang, J. H.: Comparing clouds and their seasonal variations in 10 atmospheric general circulation models with satellite measurements, J. Geophys. Res., 110, D15S02, doi:10.1029/2004JD005021, 2005.

ACPD

10, 1559–1593, 2010

Table 1. Grid Box mean ISCCP cloud properties for each cluster.

	1 – Small Cu	2 – Large Cu	3 – Sc/St	4 – Deep As	5 – Cirrus	6 – Weak Frontal	7 – Strong Frontal
Cluster Frequency (%)	27.5	18.4	16.5	14.0	11.3	7.7	4.3
Mean Cloud Fraction (%)	54.1	77.8	92.9	97.5	87.4	99.0	99.4
Mean Cloud Top Pressure (mb)	658.2	781.0	776.4	584.3	431.8	382.6	347.6
Mean Cloud Optical Thickness	3.63	2.89	7.19	8.30	2.30	8.90	23.08

ACPD
10, 1559–1593, 2010

Table 2. Grid box mean ISCCP cloud radiative forcing for each cluster.

	1 – Small Cu	2 – Large Cu	3 – Sc/St	4 – Deep As	5 – Cirrus	6 – Weak Frontal	7 – Strong Frontal
SWCRF (W/m^2)	−39.01	−40.46	−96.96	−112.89	−55.04	−123.05	−168.38
LWCRF (W/m^2)	14.81	10.32	13.17	40.59	46.71	78.26	87.02

ACPD
10, 1559–1593, 2010

Table 3. Mean surface-reported cloud properties for each cluster (Northern Hemisphere only), along with anomaly from the average over all clusters.

Observation		Cluster #						
		1	2	3	4	5	6	7
Clear-sky Frequency (%)	Mean	6.8	2.2	1.1	0.4	3.5	0.4	0.2
	Anom	3.7	−0.9	−2.0	−2.6	0.4	−2.7	−2.9
Obscured-sky Frequency (%)	Mean	2.2	2.1	10.5	9.3	1.8	9.1	12.5
	Anom	−3.3	−3.4	5.0	3.8	−3.8	3.6	6.9
Total Cloud Amount (%-sky-cover)	Mean	58.2	68.5	87.1	90.7	67.4	92.6	95.9
	Anom	−16.5	−6.3	12.4	15.9	−7.4	17.9	21.1
Low-level Cloud Amount (%-sky-cover)	Mean	47.2	59.7	79.9	80.9	48.7	79.9	86.4
	Anom	−16.6	−4.1	16.1	17.1	−15.1	16.1	22.6
Rain and Snow Frequency (%)	Mean	4.2	6.4	4.6	11.5	3.0	13.1	30.1
	Anom	−3.3	−1.1	−2.9	4.0	−4.5	5.6	22.6
No-low-cloud Frequency (%)	Mean	16.3	6.4	4.9	4.7	17.8	5.6	3.9
	Anom	6.2	−3.7	−5.3	−5.4	7.7	−4.5	−6.2
Small Cumulus Frequency (%)	Mean	18.5	13.7	5.1	4.5	15.7	4.7	2.5
	Anom	7.1	2.3	−6.3	−6.9	4.4	−6.7	−8.8
Moderate and Large Cumulus Frequency (%)	Mean	16.8	18.6	6.9	6.5	14.1	5.8	3.8
	Anom	4.7	6.5	−5.3	−5.7	1.9	−6.4	−8.3
Mixed Cumulus and Stratocumulus Frequency (%)	Mean	16.9	22.5	20.2	19.3	18.8	18.1	12.3
	Anom	−1.8	3.7	1.5	0.6	0.1	−0.6	−6.4
Ordinary Stratocumulus Frequency (%)	Mean	9.6	18.6	20.6	18.3	12.1	16.7	13.7
	Anom	−4.4	6.5	6.6	4.4	−1.8	2.8	−0.3
Fair-weather Stratus Frequency (%)	Mean	5.5	5.8	15.4	15.7	6.3	16.2	17.9
	Anom	−4.6	−4.3	5.2	5.6	−3.9	6.1	7.8
Bad-weather Stratus Frequency (%)	Mean	6.1	7.5	11.4	16.0	6.2	18.5	28.0
	Anom	−4.5	−3.2	0.8	5.4	−4.4	7.9	17.3

ACPD
10, 1559–1593, 2010

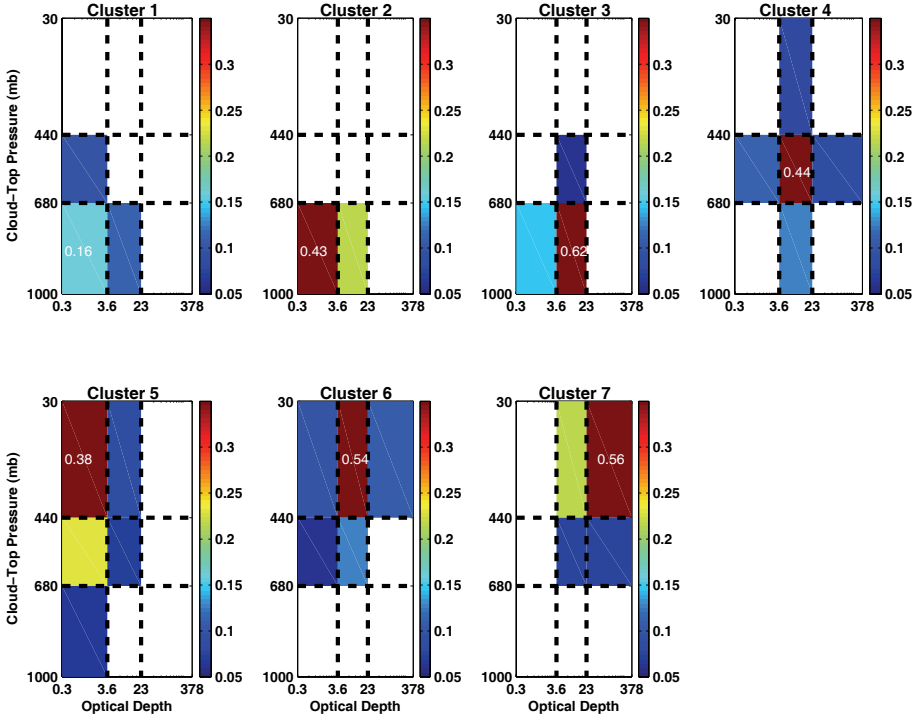

Fig. 1. Mean ISCCP histograms of cloud fraction for each cloud-top pressure and cloud optical thickness interval.

ACPD
10, 1559–1593, 2010

Cluster analysis of midlatitude oceanic cloud regimes

N. D. Gordon and J. R. Norris

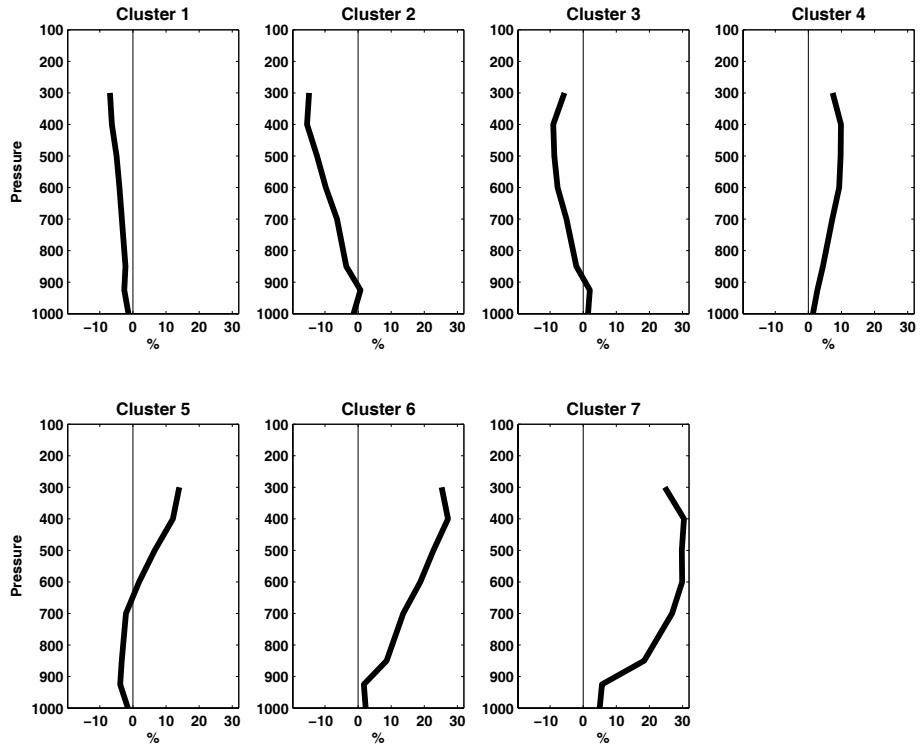

Fig. 2. Vertical profiles of mean perturbation relative humidity for each cluster from the NCEP Reanalysis.

ACPD
10, 1559–1593, 2010

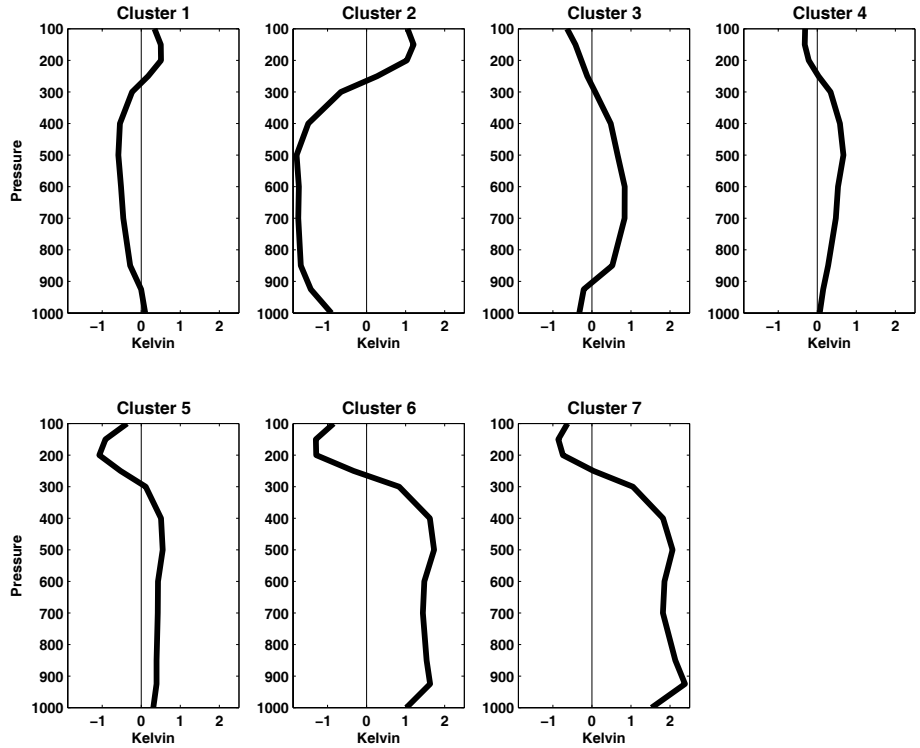

Fig. 3. As in Fig. 2, except for perturbation temperature.

ACPD
10, 1559–1593, 2010

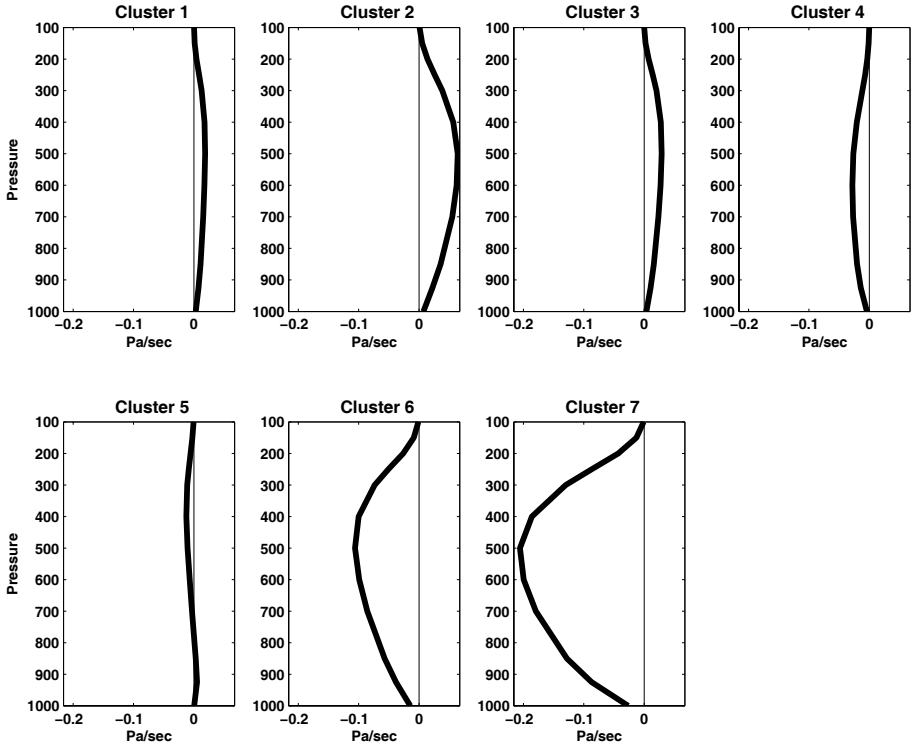

Fig. 4. As in Fig. 2, except for perturbation pressure vertical velocity.

ACPD
10, 1559–1593, 2010

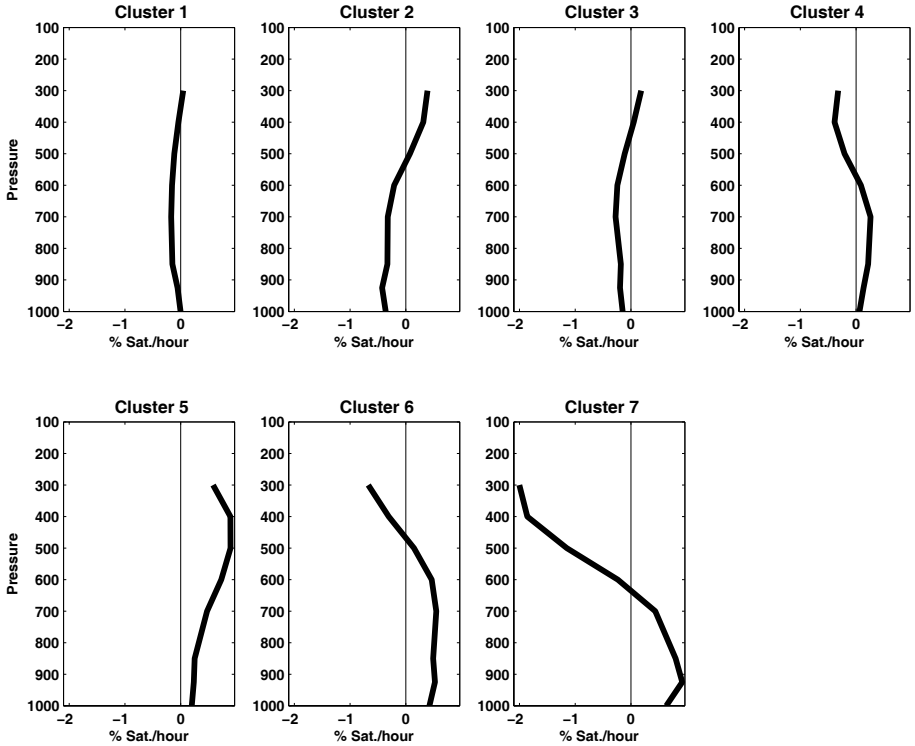

Fig. 5. As in Fig. 2, except for perturbation horizontal moisture advection.

ACPD
10, 1559–1593, 2010

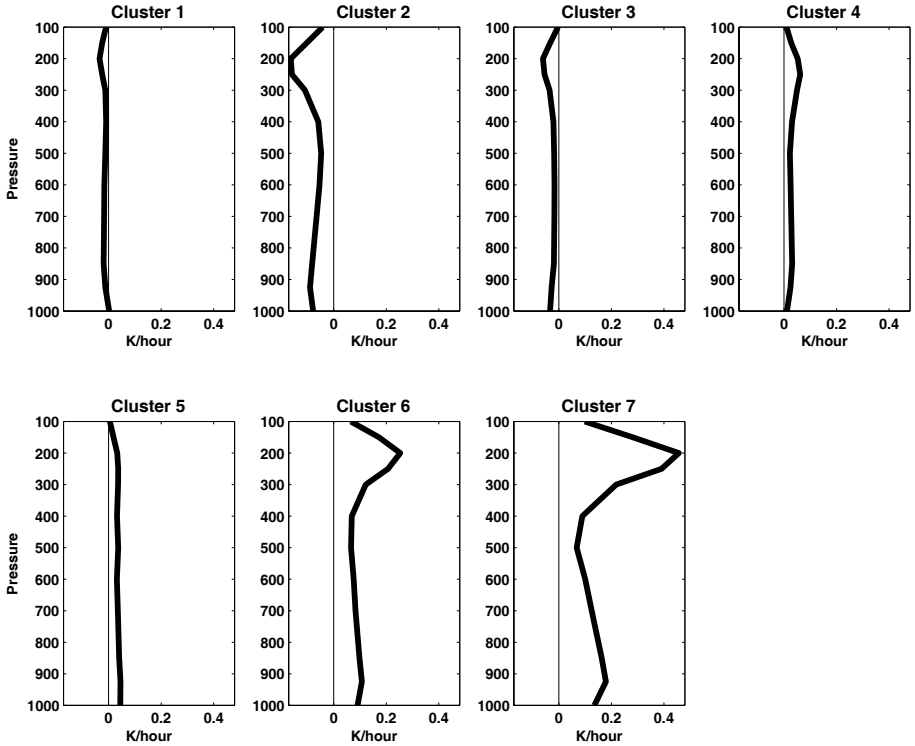

Fig. 6. As in Fig. 2, except for perturbation horizontal temperature advection.

ACPD
10, 1559–1593, 2010

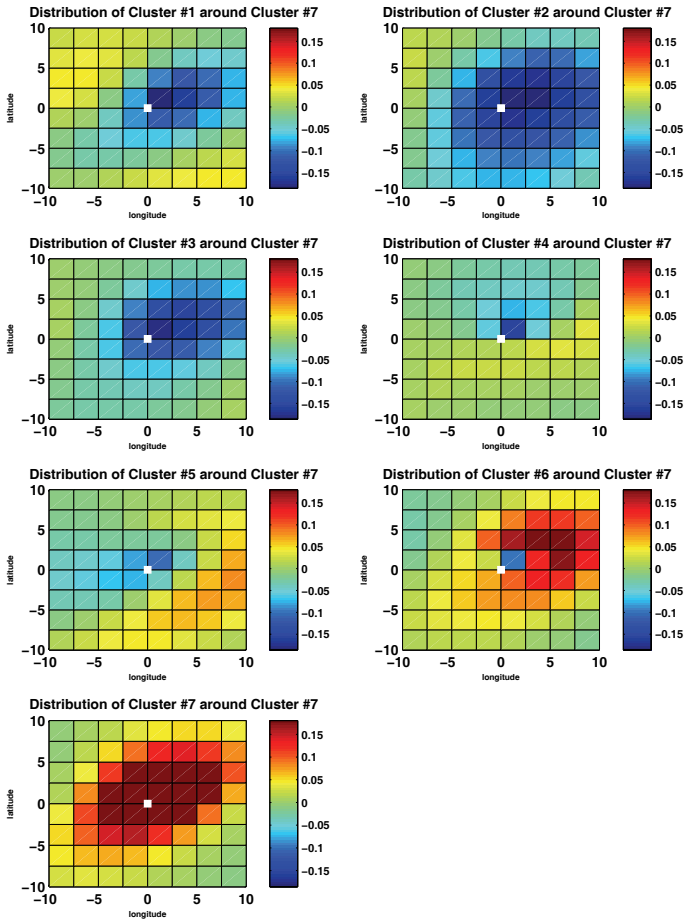

Fig. 7. Composite spatial distributions of the perturbation frequency of each cluster around a central grid box with the Strong Frontal cluster.

ACPD
10, 1559–1593, 2010

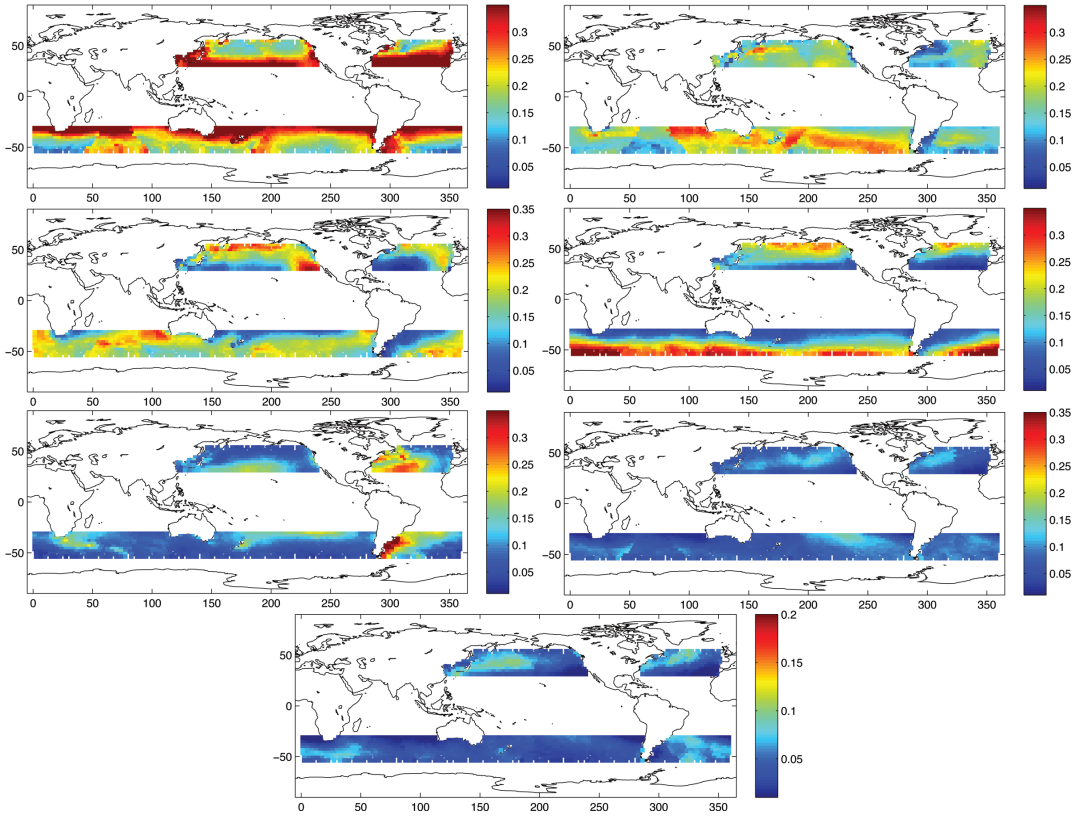

Fig. 8. Annual mean climatological spatial distributions of the frequency of each cluster.

ACPD

10, 1559–1593, 2010

Cluster analysis of midlatitude oceanic cloud regimes

N. D. Gordon and J. R. Norris

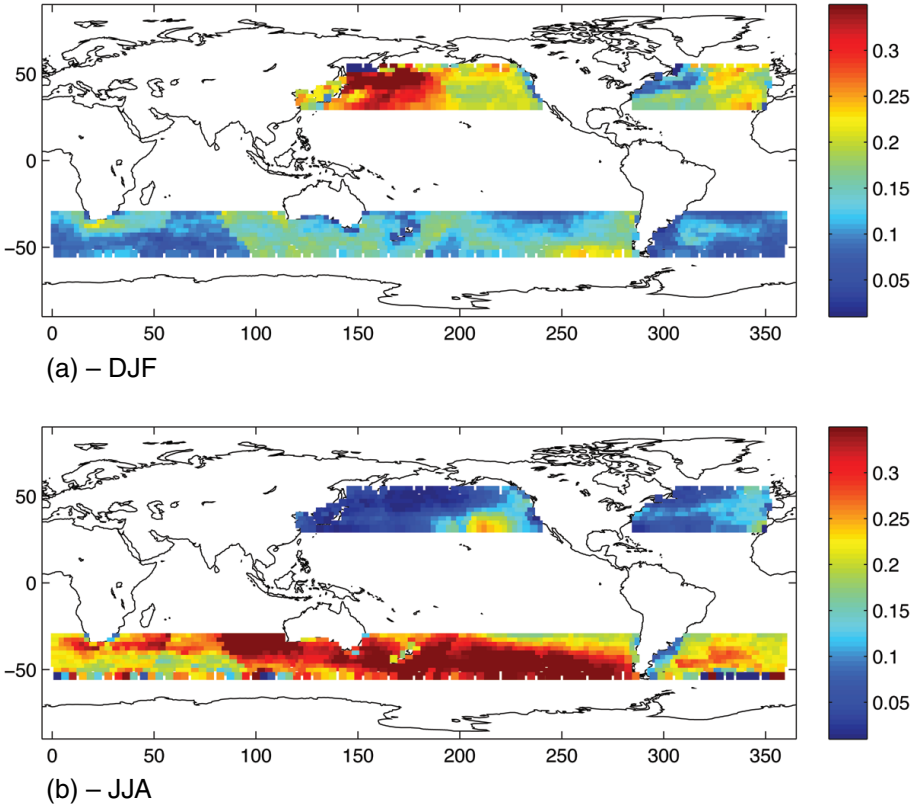

Fig. 9. Seasonal mean climatological spatial distributions of the frequency of Cluster 2 (Large Cumulus).

ACPD
10, 1559–1593, 2010

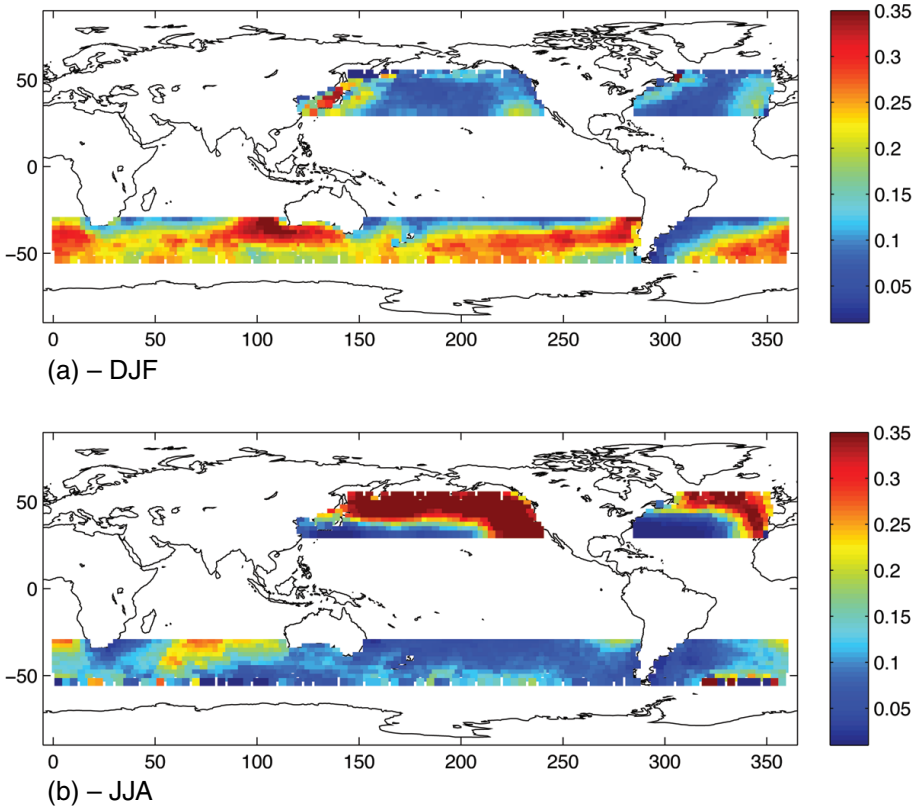

Fig. 10. As in Fig. 9, except for Cluster 3 (Stratocumulus/Stratus).

ACPD
10, 1559–1593, 2010

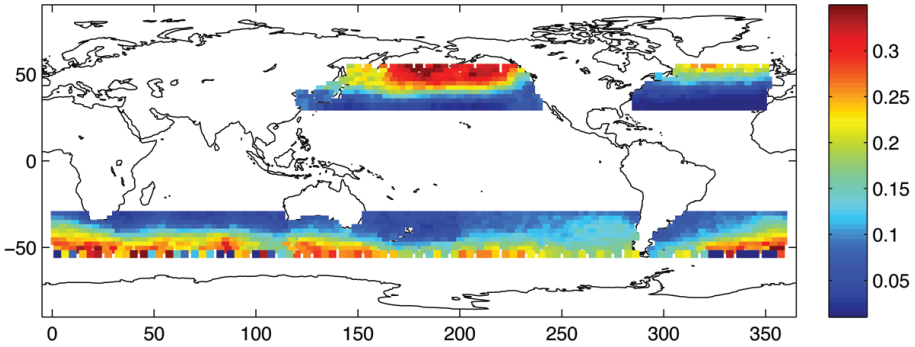

Fig. 11. JJA mean climatological spatial distribution of the frequency of Cluster 4 (Deep Altostratus).

ACPD
10, 1559–1593, 2010

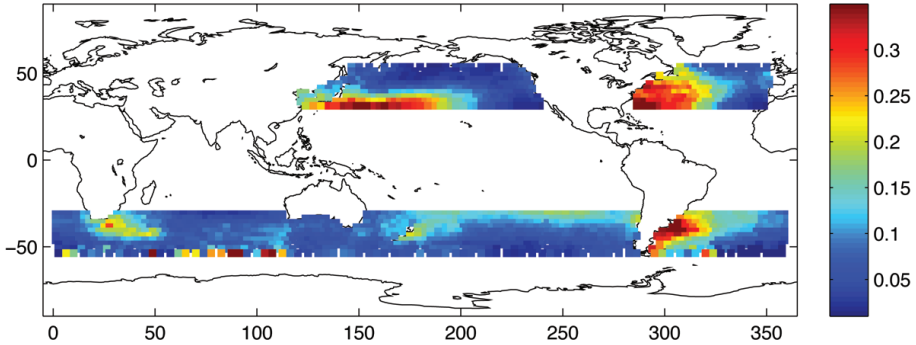

Fig. 12. As in Fig. 11, except for Cluster 5 (Cirrus).

ACPD
10, 1559–1593, 2010